Supramolecular assembly of Ce^{IV}-oxo sulfate torus with transition metal countercations

Ian Colliard and May Nyman[*]

Department of Chemistry, Oregon State University, Corvallis, OR 97331, USA

*correspondence: may.nyman@oregonstate.edu

Abstract

M^{IV} molecular oxo-clusters of the *f*- and *d*-block (M=Zr, Hf, Ce, Th, U, Np, Pu) have been prolific in bottoms-up material design, catalysis, as well as understanding metal oxide assembly, dissolution and surface reactivity in nature and in synthesis. Here we introduce Ce$_{70}$, a new Ce^{IV} wheel-shaped oxo-cluster, $[Ce^{IV}(OH)_{36}(O)_{64}(SO_4)_{60}(H_2O)_{10}]^{4-}$, isostructural with prior-reported U$_{70}$. Like U$_{70}$, Ce$_{70}$ crystallizes into intricate frameworks with divalent transition metal countercations (TM^{II}), and also Ce^{IV}-monomer and sulfate addenda ions. Eight structures are described by single-crystal X-ray diffraction that feature four framework types, named to describe the arrangement of the Ce$_{70}$-rings. These include the propeller framework (with Co^{II} and Zn^{II}), the offset-stacking framework (with Ni^{II} and Cd^{II}), the tartan framework (with Co^{II} and Cu^{II}), and the isolated framework (with Co^{II} and Zn^{II}). Small-angle X-ray scattering studies of dissolved Ce$_{70}$ shows they undergo offset stacking or eclipsed stacking in solution, depending on the monomer cations. Larger TM^{II} promote eclipsed stacking, whereas, Ce^{IV} inhibits eclipsed stacking. To these organic solutions, we have added alkaline earths, Mn^{II} and Ce^{IV} to provide direct evidence for their role in solution phase supramolecular assembly. This study opens the door to discovery of mixed Ce$^{III/IV}$ oxo-clusters important in catalysis, other members of the M$^{IV}_{70}$ family (i.e. Pu^{IV}), new clusters for metal-organic framework design, and assembly into functional surfaces.

Introduction

Metal-oxo clusters can be considered molecular metal oxides. They are both aesthetically fascinating and fundamentally useful in geosciences, environmental science and materials science. For example, they provide a foundation to understand metal oxide dissolution and precipitation in nature and in synthesis.[1-8] The atomic precision of metal-oxo clusters allows investigation of chemical processes of non-molecular counterparts including surfaces, bulk materials and

nanoparticles.[9-11] Additionally, metal-oxo clusters function as single-molecule magnets and catalysts, linked into frameworks and supramolecular assemblies, as well as isolated clusters.[12-21] Supramolecular assembly of metal-oxo clusters creates another level of complexity and emergent properties in fractals, superlattices and nanomaterials.[22-26]

Cerium oxide clusters and nanomaterials are of special relevance. Owed to the facile Ce^{III}-Ce^{IV} redox behavior and concomitant oxygen transport, ceria nanoparticles are used as automotive redox catalysts, in oxide fuel cells, and as photoactive solar cell materials.[27-29] Performance efficiency of cerium oxide nanoparticles is correlated to the presence of Ce^{III} and oxygen-vacancies on the surface.[27, 30] As such, it is difficult to control the composition, size, and structure of cerium nanoparticles.[31, 32] Moreover, determining cerium oxidation state in molecules via simple bond valence sum calculations is particularly challenging, for reasons not well-understood.[33] Thus, characterization of such species to identify and exploit structure-property relationships remains a challenge. However, like most large tetravalent metals of the d- and f-blocks (M^{IV} = Zr, Hf, Ce, Th, U, Np, and Pu), molecular Ce^{IV}-oxo molecular clusters resembling the oxide framework in both structure and function can be isolated. The most common structural motif of these tetravalent metal oxo-clusters is the hexamer (Ce_6, $[M_6^{IV}(OH)_4(O)_4]^{12+}$),[34-40] that is ligated and stabilized via carboxylate, nitrate, sulfate, and polyoxometalate (POMs) ligands.[41-46] Ce_6 hexamers are quite prolific in the literature, including linked into metal-organic frameworks.[34, 47-54]

Beyond the hexamer, larger Ce^{IV}-oxo clusters have been isolated from organic media, and these usually contain and are built symmetrically around a Ce_6 core, and by extension resemble ceria. These cluster nuclearities include Ce_{10}, Ce_{20}, Ce_{22}, Ce_{24}, Ce_{38} and Ce_{40}, of which Ce_{10}, Ce_{22}, Ce_{24}, and Ce_{40} have distinct Ce^{III} and Ce^{IV} sites.[44, 55] As an additional focus of Ce-oxo clusters, Ce^{IV} is an important surrogate for Pu^{IV}, given its similar radius and observed species formation.[44, 56] In oxo-cluster chemistry, Pu^{IV}_{38} and Pu^{IV}_{22} analogues to Ce_{38} and Ce_{22} have been synthesized.[9, 56-58] Because the Ce_{22} cluster contains both Ce^{III} and Ce^{IV}, while Pu_{22} contains exclusively Pu^{IV}, we recognize the potential for structural and compositional flexibility of M^{IV} oxo-clusters in general. Isolating mixed oxidation state or heterometal oxo-clusters represents enormous potential in tuning electronic, structural and chemical properties.
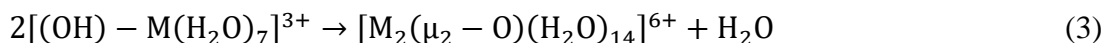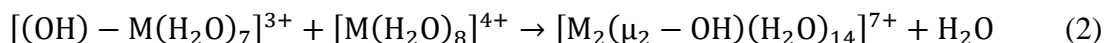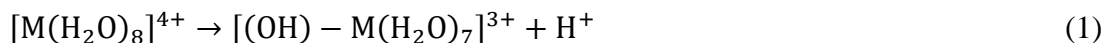
Recently we exploited sulfate ligation and high oxidation state counter-cations (lanthanides and transition metals, Ln^{III} and TM^{II}) to isolate a new family of giant U^{IV} oxo-clusters including the U_{84} 'superatom' (with Ln^{III}) and U_{70} wheel structure (with TM^{III}).[26, 59] In addition to

contributing to understanding solution and solid phase supramolecular assembly processes, U/Pu^{IV}-sulfate speciation is of special interest from the standpoint of geochemical fate and transport. Bacteria can immobilize U^{IV} through the oxidation of sulfur. Environmental fate of Pu is less known,[60] but metal-oxo clusters such as U/Pu$_{38}$ are excellent surrogates for colloidal U/Pu oxides in the geobiosphere. As an intermediate step to expanding Pu^{IV} oxo-cluster chemistry and broadening knowledge across the actinide series, we have translated TM^{II}/Ln^{III}-U^{IV}-sulfate speciation to Ce^{IV}-sulfate chemistry.

Herein, we introduce the Ce$_{70}$-sulfate family with divalent transition metal counter-cations (Co^{II}, Zn^{II}, Ni^{II}, Cd^{II}, Ni^{II}, Cu^{II}), and unveil some distinct differences from the original U$_{70}$-sulfate family. First, due to the redox stability of Ce^{IV} under applied synthetic conditions, we were not hindered by redox activity of the transition metals. Second, the transition metals play a more significant role in supramolecular assembly in solid-state frameworks and upon re-dissolution in organic solvents. Third, Ln^{III} also isolates the Ce$_{70}$-ring, but will be presented in a later publication. In both the U^{IV} and Ce^{IV} families, M^{IV} monomers also participate in solid-phase assembly. Cerium is the second member to join the M$^{IV}_{70}$ family and represents the largest Ce-oxo cluster to date. Via eight X-ray crystal structures, we show four distinct framework assembly types, and X-ray scattering reveals the role of the TM^{II} counter-cations on solution-phase assembly.

Results and Discussion

Highly-charged metal cations complex aqua ligands upon dissolution, followed by deprotonation, even in acidic conditions, leading to oligomerization. If uncontrolled, the end-product of this reaction is metal oxide precipitation. The addition of heterometal cations and strongly coordinating oxoanion ligands mediate the fundamental hydrolysis (1) and condensation reactions (olation (2) and oxolation (3)) that drive oligomerization.

$$[M(H_2O)_8]^{4+} \rightarrow [(OH) - M(H_2O)_7]^{3+} + H^+ \tag{1}$$

$$[(OH) - M(H_2O)_7]^{3+} + [M(H_2O)_8]^{4+} \rightarrow [M_2(\mu_2 - OH)(H_2O)_{14}]^{7+} + H_2O \tag{2}$$

$$2[(OH) - M(H_2O)_7]^{3+} \rightarrow [M_2(\mu_2 - O)(H_2O)_{14}]^{6+} + H_2O \tag{3}$$

Moreover, counter-cations play primary roles in the assembly of any oligomeric species in the crystallization process.[61-64] Combining first-row transition metals with Ce^{IV}(SO$_4$)$_2$ and heating at

75 °C (see SI for details) promotes assembly of the Ce_{70} torus cluster; fully formulated $[Ce^{IV}(OH)_{36}(O)_{64}(SO_4)_{60}(H_2O)_{10}]^{4-}$, isostructural with prior reported U_{70} (**Figure 1a**).[26, 59] Analogous to U_{70}, the Ce_{70} cluster can be viewed as alternating Ce_6 and Ce_1; four sulfates bridge a Ce_6 and a Ce_1 along the outer rim, and four additional sulfate line the inner rim bridging only between Ce_6, see Figure 1b.[59] The entirety of the ring exhibits O/OH disorder, as determined by bond valence sum calculations. Most Ce-centers are 8-coordinate, with the exception of the innermost Ce of the Ce_6 unit that is capped by an additional water molecule. Charge of the Ce was confirmed by bond valence sum (BVS), see Table S12 for a representative example amongst the eight structures. Ce BVS values ranges from 3.62-4.00 (average=3.88). The bond length ranges include: Ce – OH^-/O^{2-} = 2.11 – 2.67 Å, Ce – OH_2 = 2.28 Å – 2.80 Å, and Ce-OSO_3 = 2.30 – 2.99 Å. Oxygens with a BVS around 2.0 were assigned as O^{2-}, those with BVS~1.0 were assigned as purely OH^-, and those with BVS in between were assigned as mixed OH^-/O^{2-}. Addenda sulfates, along with TM^{II} and Ce^{IV} monomers, decorate and bridge the Ce_{70} rings (Figure 1c), defining different Ce_{70}-framework patterns.
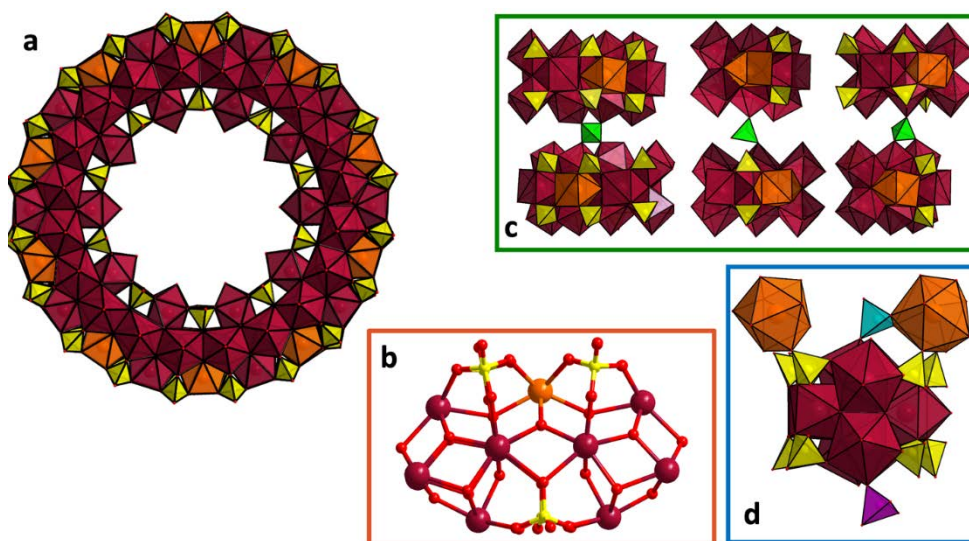
Figure 1. Summary of species that comprise **Ce_{70}-frameworks** A) Polyhedral representation $[Ce_{70}(OH)_{36}(O)_{64}(SO_4)_{60}(H_2O)_{10}]^{4-}$, the Ce_6 unit is maroon and the Ce_1 is orange, sulfate is yellow. B) Ball-and-stick representation of a fragment of Ce_{70}, emphasizing the sulfate bridging between Ce_6 on the inside (towards the bottom) and outside (top) between Ce_1 and a Ce_6. C) Polyhedral representation of addenda sulfates (green) bridging between Ce_{70} rings, based on its connectivity. Left to right 'edge-to-edge', 'corner-to-corner', and 'edge-to-corner'. D) Binding modes of addenda Ce^{IV}-monomers to both Ce_{70}-sulfates and addenda sulfates. Sulfates integral to the Ce_{70}-ring are yellow. The addenda sulfate that chelate a Ce^{IV}-monomers are turquoise, non-bridging addenda sulfates are pink.

Individual TM^{II} bonding behaviors and the synthesis conditions leads to four unique architectural assemblies of the Ce$_{70}$ plus Ce^{IV}-monomer/TM^{II}-counterions, and addenda sulfates, and will be described in detail later. Based on arrangement of the Ce$_{70}$-rings, these are dubbed 1) propeller framework, 2) standard offset-stacking, 3) tartan, and 4) isolated rings. The prior described U$_{70}$-family, on the other hand, only featured the standard offset-stacking arrangement. A major difference between the Ce$_{70}$-family and the U$_{70}$-family is the prevalence of Ce^{IV}-monomer that serve as counterions for the former. This additional building unit endows the Ce$_{70}$-family with more diverse supramolecular assembly patterns.

Here we consider the effect of reaction conditions and TM^{II} cation properties on framework assembly. These include TM^{II} concentration, TM^{II} coordination behavior, and pH of the reaction solution. Metal cation concentration in water and charge-to-size ratio (charge density) mediates pH by processes outlined in equations 1-3. Hypothetically, increased metal concentration and charge-density of the metal cations decrease pH. However, for all reaction solutions with different TM^{II} and different concentrations of TM^{II}, the pH before and after hydrothermal treatment is 1.5 and 2.5, respectively, suggesting pH has minimal influence on framework assembly. We can also assume that in these reaction conditions, the higher valence Ce^{IV} controls acidity, not the divalent transition metals.

One clear correlation is the influence of TM^{II}-concentration on framework arrangement (see synthesis details in the SI). For example, the propeller and offset-stacking frameworks crystallize optimally from the lowest TM^{II}-acetate concentration of approximately 0.15 mmol. Increasing the TM^{II} concentration to 0.20 mmol introduces the tartan framework. From a 0.40 mmol concentration of TM^{II}, the isolated framework is favored. Counterintuitively, increasing the TM^{II} concentration in the reaction solution leads to an increase in Ce^{IV}-monomer incorporation into the framework (accompanied by decreased TM^{II} incorporation). The extreme case is the isolated framework in which the Ce$_{70}$ rings are completely rimmed and separated by Ce^{IV}-monomers. We attribute this unexpected trend to the role of the transition metals on the Ce$_{70}$-formation process. When present in high concentration, transition metals could slow Ce$_{70}$-formation, leading to an abundance of Ce^{IV}-monomers during framework assembly and crystallization processes.

To identify trends in Ce^{IV}/TM^{II} monomer incorporation and their influence on framework type, we have compiled detailed bonding information of these monomers for the reported eight

structures (**Table 1**). Included in this assessment is a parameter describing ligation of the monomers by water vs. by sulfate, termed the weighted average (W.A):

$$W.A. = \frac{\Sigma(S.O.F._{monomer} * N_{monomer} \; aqua \; ligands)}{\Sigma(S.O.F._{monomer} * N_{monomer} \; total \; coordination)} \qquad (4)$$

The structure occupancy factor (S.O.F., Table S9) is accounted due to different occupancies of these monomer sites, ranging from 0.25 to 1.0, and different ligation; similar to the prior-reported U_{70} frameworks.[26, 59] A W.A. value of 1.0 will describe the collective cation monomers (every monomer regardless of S.O.F.) to be fully coordinated by aqua ligands. Increasing sulfate coordination decreases the W.A. value. In general, a lower W.A. describes more extensive monomer-sulfate-monomer linkages within the framework. Differences in W.A. can be seen by changing TM^{II} (see propeller structures) or by changes in family (see $CoCe_{70}$ series), however distinct trends without exceptions are difficult to identify. Similar to the prior reported U_{70} structures, Zn is unique in its strong preference for bonding to water over bonding to sulfate, promoting formation of the isolated framework with extensive incorporation of Ce^{IV}-monomer bonding to Ce_{70}.[26, 59] Additionally, for the Ce^{IV}-monomer, tracking of sulfate ligation can also be seen by the coordination mode for the ligands. There's a notable shift in the coordination of the monomers, highlighted by the number of monodentate (pink in figure 1d) and the chelating sulfates (turquoise in figure 1d), see also Table 1. The most dramatic change is from use of a second row transition metal, Cd^{II}, which crystallizes Ce_{70} as the offset-stacking framework. This structure is the only one reported that contains no Ce^{IV}-monomers. The rich variety of obtained frameworks as a function of the specific transition metal and its concentration, as well as the effect of the incorporated Ce^{IV}-monomer highlights the complex role of countercations in stabilizing large metal-oxo polyanions, and in the framework assembly thereof. The four different frameworks types are described in detail below, highlighting these roles.

Table 1. Summary of the coordination environment of Ce^{IV} and TM^{II} monomers in reported structures

TM^{II}-Framework type	Radii of TM^{II} (and Ce^{IV}) (Å)[2]	TM^{II}- (H_2O) W.A.[1]	Ce^{IV}- (H_2O) W.A.[1]	# Monodentate (SO_4)-Ce^{IV} [3,4]	# Chelating (SO_4)-Ce^{IV} [3,5]	Monomer Ratios Ce^{IV}:TM^{II} [3]
$CoCe_{70}$-propeller	0.89	0.75	0.70	3	0	3.00
$ZnCe_{70}$-propeller	0.88	1.00	0.66	3	1	2.50
$NiCe_{70}$-offset stacking	0.83	0.67	0.67	2	1	0.33
$CdCe_{70}$-offset stacking	1.09	0.70	-	-	-	-
$CoCe_{70}$-tartan	0.89	0.88	0.56	2	1	0.50
$CuCe_{70}$-tartan	0.87	0.67	0.56	2	1	2.00
$CoCe_{70}$-isolated	0.89	1.00	0.56	2	2	4.50
$ZnCe_{70}$-isolated	0.88	1.00	0.54	2	2	9
Ce^{IV}-monomer	1.01					

[1]*The weighted average of the hydration of each monomer, see Table S9 and equation 4.*
[2]*6-coordinate radius[65]*
[3]*per formula unit*
[4]*yellow sulfates in figure 1d*
[5]*turquoise sulfates in figure 1d*

Ce_{70}-propeller Framework

The 'larger' first row TM^{II} at lower concentrations favor the 'propeller' framework. $CoCe_{70}$-propeller, formulated $CoCe_3Ce_{70}(OH)_{36}(O)_{64}(SO_4)_{65}(H_2O)_{65.5}$ (Table S1), crystallizes in the monoclinic $P2_1/c$, space group (V = 31,298 Å^3). The structure features the Ce_{70} stacking in an offset manner along the a-axis, reminiscent of the U_{70} frameworks. The rings are bridged by two $S(\mu_1$-O$)_4$ or 'edge-to-edge' sulfates, four Ce^{IV} centers apart within the ring, making chains (see Figure 1c for sulfate coordination). This is consistent with stronger linking compared with the U_{70}-frameworks, which bridged via corner-to-corner linked sulfate. Additional addenda sulfates decorate the ring, charge balancing the Ce^{IV}- and Co^{II}-monomers. The Ce^{IV}-monomers direct Ce_{70}-linking in the propeller arrangement via skewed linking (figure 2a). Two fully-occupied Ce^{IV}-monomer sites (Ce33), related by an inversion center across the ring, bridge one Ce_{70} to two pairs of neighboring Ce_{70} rings on opposite sides of the central ring. These neighboring Ce_{70} and their chains rotate ~45° from the plane of the middle Ce_{70} chain, driving the propeller-shaped connectivity (figure 2a, Ce33 is top and bottom of the central ring). The Ce33-monomer bridges a total of three rings and is 9-coordinate with a tricapped-trigonal prismatic geometry (figure 2c). Approximately a quarter way around the ring from Ce33 is an additional Ce^{IV}-monomer (Ce37)

disordered over two positions (occupancy = 0.5, positions on the left and right of the central Ce_{70} in figure 2a). This monomer bridges the chains approximately along the *b*-axis, reinforcing a three-dimensional framework (Figure S1b). Partially occupied Co^{II}-monomers also participate in framework-linking, either by direct bonding of Ce_{70}-sulfate and addenda sulfate, or H-bonding to sulfates through coordinated aqua ligands. Co^{II} exhibits an octahedral geometry, with four to five aqua ligands (Figure S1).
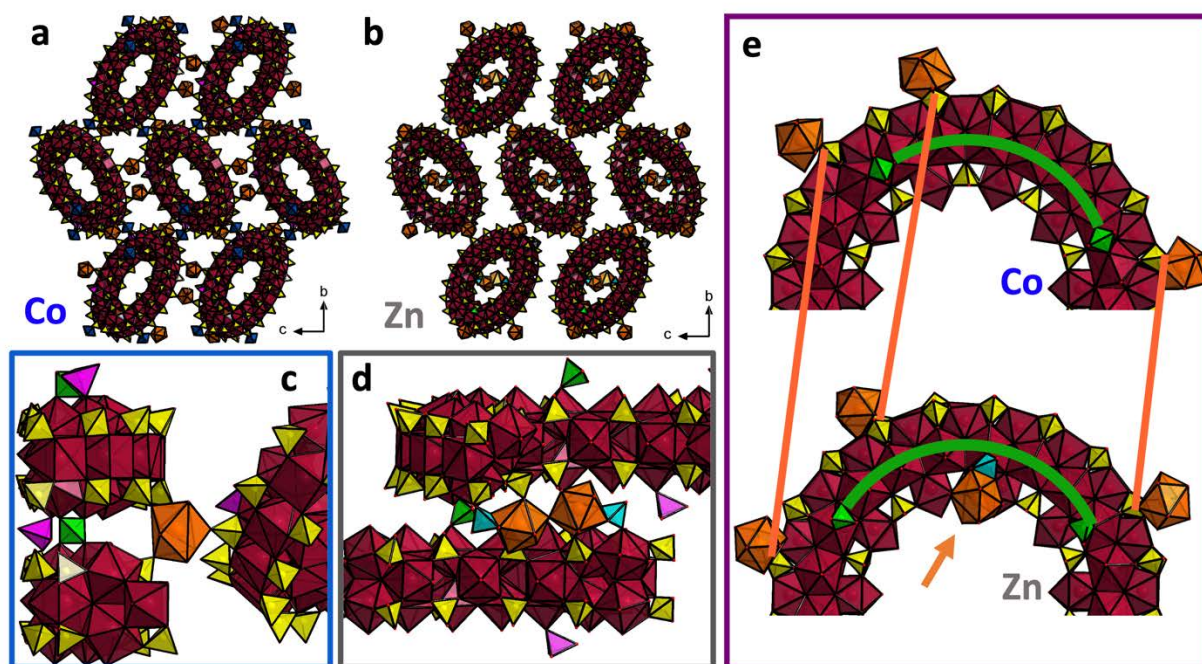
Figure 2. **Polyhedral representation the propeller-framework.** a) stacking view of $CoCe_{70}$-propeller along *a*-axis; b) stacking view of $ZnCe_{70}$-Propeller along *a*-axis; c) view highlighting connectivity of the linking Ce^{IV}-monomer (Ce33), joining three Ce_{70} in $CoCe_{70}$; d) view of the inter-ring connectivity with the positional disordered Ce monomer (Ce37) for $CoCe_{70}$; e) $CoCe_{70}$ and $ZnCe_{70}$ rings showing shifts in the location of the Ce^{IV}-monomers and the ring-bridging sulfates. The corresponding colored lines highlight the shifts in position of the sulfates and the Ce^{IV}-monomers, and the green arc scribes the distance between the ring-bridging sulfates. Ce-polyhedra of Ce_{70} are maroon, Ce^{IV}-monomers are orange polyhedra, Ce_{70} sulfates are yellow, addenda sulfate in pink, ring bridging sulfates are green, chelating sulfates are light blue, Co^{II} monomers in blue, Zn^{II} monomers are grey.

The $ZnCe_{70}$-propeller framework (figure 2b), formulated $[Zn(H_2O)_6]Ce_{2.5}Ce_{70}(OH)_{36}(O)_{64}(SO_4)_{64}(H_2O)_{58.5}$ (Table S2), crystallizes in the triclinic *P*-1 space group (V = 38,040 $Å^3$). Similar to the $CoCe_{70}$ analogue, this structure features the Ce_{70} rings stacked in an offset fashion along the *a*-axis. However, there is a loss in framework symmetry and connectivity, which comes from the diminished participation of Zn^{II} in the framework formation. Zn^{II}-monomers are fully-coordinated by aqua ligands, charge balancing the framework and

interacting between neighboring Ce_{70} rings and chains via H-bonding (figure S2). Balancing the loss of Zn^{II}-OSO_3 bonding, there is an increase in Ce^{IV}-OSO_3 ligation, via increase of chelating-bridging sulfates to the Ce^{IV}-monomers, see Table 1. In the $ZnCe_{70}$-propeller framework, the rings are bridged by two $O_2S(\mu_1$-$O)_2$ or 'corner-to-corner' sulfates, spanning six Ce^{IV}-centers apart around the ring (Figure 1c and 2e). The decrease in offset along the a-axis stacking, and inter-ring distance accommodates the addition Ce^{IV}-monomer locations and chelating sulfate. Two disordered cerium monomers (Ce72 and Ce74, each disordered over two half-occupied positions) are located in the inner void of the torus, bridging between rings within a chain (figure 2d). The loss of symmetry comes from the diverging location of the monomers located around the ring. Due to increase in ring offset of the Zn-analogue, the anchoring position of the Ce^{IV}-monomer also shifts. The shift causes the ring to rotate with respect the ~45°˙ torsional (figure 2e). Unlike the Co-analogue, the inter-chain bridging Ce^{IV}-monomers (Ce71 and Ce73) exhibit reduced site occupancy (75%). The overall loss of symmetry and framework connectivity is consistent with zinc's diminished role in framework formation (figure S2).

Ce_{70}- offset-stacking framework

The **$NiCe_{70}$-offset-stacking** framework, formulated $Ni_3CeCe_{70}(OH)_{36}(O)_{64}(SO_4)_{63}(H_2O)_{63}$ (Table S3), crystallizes in the triclinic P-1 space group (V = 16,197 $Å^3$). By preliminary structure determination, an isomorphic Cu-analogue was also obtained, but only the Ni structure will be discussed here. As the main feature of all the U_{70} and Ce_{70} frameworks, the rings stack in an offset manner along the a-axis. The rings are bridged in the stacking direction by two $OS(\mu_1$-$O)_3$ or 'edge-to-corner' sulfates, five Ce^{IV} centers apart (figure 1c shows the sulfate bonding modes). The location of the Ce^{IV}-monomer is similar to the $ZnCe_{70}$-propeller framework, where it bridges via a chelating sulfate inside the void of the rings, reinforcing the chain. All Ni^{II}-monomers are 6-coordinate, with four aqua ligands and *trans*-bridging monodentate sulfates (figure S3). The Ni^{II}-monomers serve to bridge chains together, and uniquely bridge rings within the chains (Figure 3a). However, the distorted octahedral geometry of the d^8 Ni^{II} may be viewed as square planar, and not coordinated to the framework. The *trans* Ni-OSO_3 bonds are elongated (2.498 – 2.521 Å), in comparison to the aqua ligands, Ni – OH_2 1.941 – 1.997 Å. The O_3SO-Ni-OSO_3 bond angle is also bent (164°) (Table S10 and figure 3b).

The **CdCe₇₀-offet-stacked** framework, formulated $Cd_7Ce_{70}(OH)_{36}(O)_{64}(SO_4)_{65}(H_2O)_{72}$ (Table S4), crystallizes in the triclinic P-1 space group (V = 15,899 Å^3). In this framework the ring stacking along the a-axis is reinforced by two $S(\mu_1\text{-}O)_4$ or 'edge-to-edge' sulfates, four Ce^{IV}-centers apart around the ring (figure S4). The framework features no Ce^{IV}-monomers, only Cd^{II}-monomers and the corresponding addenda sulfates. The Cd^{II}-monomers are all six-coordinate with four or five aqua ligands. They link rings together within the chains along the a-axis, or between the chains, reinforcing a three-dimensional structure (Figure S4). Interestingly, CdCe₇₀ is the only framework that does not contain Ce^{IV}-monomer. This is correlated with the radius: the Cd^{II} radius is the only TM^{II} that is comparable to Ce^{IV} (Table 1)[65] suggesting the larger radii cations are strong network formers, important in the crystallization process.

Ce₇₀-tartan Framework

With higher concentration of Co^{II} in the reaction solution (0.30 mmol), **CoCe₇₀-tartan**, formulated as $[Co(H_2O)_6]_2Co_2Ce_2Ce_{70}(OH)_{36}(O)_{64}(SO_4)_{66}(H_2O)_{63}$ (Table S5), crystallizes in the monoclinic $P2_1/c$, space group (V = 34,977 Å^3). This structure does not feature the ring-bridging sulfate as seen with the previous structures. Instead, there is an increase in Ce^{IV}- and Co^{II}-monomer participation in ring-bridging, leading to unique assembly of Ce₇₀. The main structure directing sites are the Ce35 and Co2 monomers, with respective occupancy of 1.0 and 0.5 (figure 3d). These two monomers bridge neighboring Ce₇₀ rings at almost a perpendicular angle (86°), thus the stacking is reminiscent of a tartan pattern (figure 3c). The remaining Co^{II}-monomers (Co1, Co3 and Co4, all half-occupied) stabilize, and charge balance the structure. Co3 is terminally linked to sulfate of Ce₇₀ and its bound aqua ligands hydrogen-bond to neighboring Ce₇₀. Co1 and Co4 are fully coordinated by aqua ligands and interact with neighboring Ce₇₀-rings via H-bonding only (figure S5).

CuCe₇₀-tartan, fully formulated $CuCe_2Ce_{70}(OH)_{36}(O)_{64}(SO_4)_{62.5}(H_2O)_{61}$ (Table S6), crystallizes in the monoclinic $P2_1/c$ space group (V = 37,328 Å^3). An isostructural Ni-analogue was also synthesized, but only the Cu structure is presented. The structure is roughly similar to CoCe₇₀-tartan. Like the Co-analogue, Ce^{IV}- and Cu^{II}-monomers bridge the nearly perpendicular Ce₇₀-rings with an 89° angle between connected rings. Disordered Ce^{IV}-monomers bridge the perpendicular rings on either side of the Ce₇₀ unit (figure 3e). The only two Cu-sites, Cu1 and Cu2, are positionally disordered, with an occupancy of 0.5 total (figure 4c). Compared to the Co-

analogue, the Ce^{IV}-monomers are more significant in framework formation for the $CuCe_{70}$-tartan phase (Tables 1 and S9).
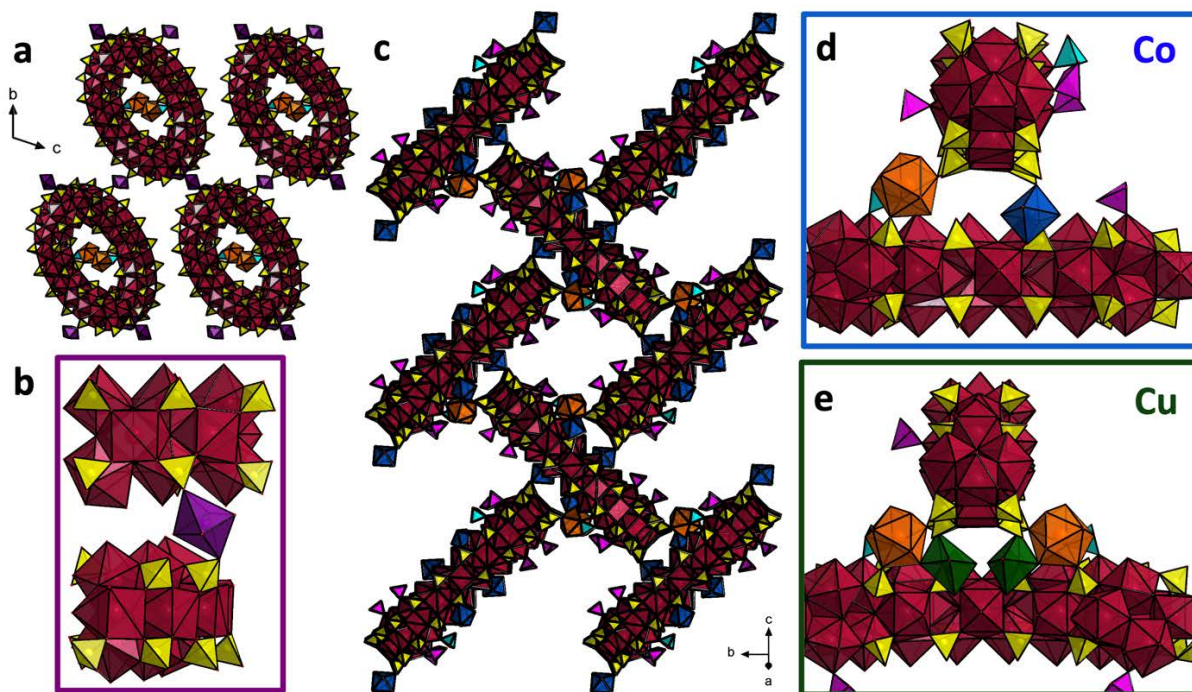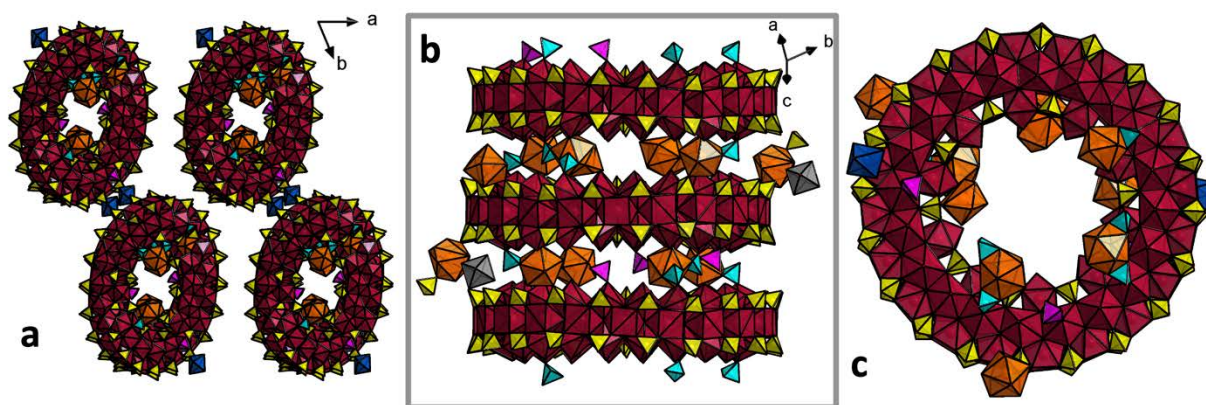

Figure 3. **Polyhedral representation the tartan and offset-stacking frameworks**. a) View along *a*-axis for $NiCe_{70}$-offset-stacking framework. b) Ni^{II}-monomer, *trans*-bridging two Ce_{70} rings within a chain. c) Quasi-perpendicular stacking of the Ce_{70} rings of the $CoCe_{70}$-tartan framework. d) Illustrating the main Ce^{IV} and Co^{II} monomer linkers of the $CoCe_{70}$-tartan framework. e) Anchoring of the two Ce_{70} rings within the tartan framework (Cu-analogue). Ce polyhedra of Ce_{70} are maroon, Ce^{IV}-monomers are orange, Ce_{70} sulfates are yellow, addenda sulfate are pink and turqoise, Co^{II}-monomers are royal blue, Cu^{II}-monomers are green, and Ni^{II}-monomers are purple.

Ce_{70}-isolated framework

Similarities between 1) the Co- and Zn-analogues of the Propeller framework, and 2) the Co- and Cu tartan frameworks, suggest the possibility of a $ZnCe_{70}$-tartan framework. However, zinc's structural history with the M^{IV}_{70} posits the opposite. X-ray absorption spectra for TM^{II}-sulfates, as well as calculated and empirical stability constants shows that Zn's full $3d^{10}$ shell, minimizes covalent contributions to bonding with sulfate, meaning sulfate-zinc bonding is less favorable.[66, 67] The tendency of Zn to coordinate simply as $[Zn(H_2O)_6]^{2+}$ has led to the discovery of a new framework type, the isolated framework (also formed with Co^{II} with higher cobalt concentration in the reaction solution). As aforementioned, we believe the higher TM^{II}

concentration (see SI, experimental) slows assembly of Ce_{70} rings, retaining more Ce^{IV}-monomers as counterions and Ce_{70} framework-linkers.

Figure 4. Polyhedral representation of the isolated frameworks (Co and Zn). a) Stacking view along c-axis for CoCe$_{70}$-isolated. b) Side view of the Ce_{70} stacking showing bridging Ce^{IV}-monomers in lieu of ring bridging sulfates. c) Ce_{70} decorated only by Ce^{IV}-monomers. Ce_{70} is maroon Ce and yellow sulfates, Ce^{IV}-monomers are orange, addenda sulfates are pink and turquoise, Co^{II}-monomers are blue, Zn^{II}-monomers are grey.

CoCe$_{70}$-isolated, fully formulated $[Co(H_2O)_6]Ce_{4.5}Ce_{70}(OH)_{36}(O)_{64}(SO_4)_{68}(H_2O)_{65}$ (Table S7), crystallizes in the triclinic P-1 space group (V = 34,915 Å^3). Ni, Cu, and Cd analogues were recognized by synthesis and structure determination, but only Co analogue will be described here. Like the tartan framework, there are no sulfate bridges between the rings (figure 4b). The Ce_{70} stacks offset approximately along the c-axis, similar to the earlier frameworks. In these structures, only the Ce^{IV}-monomer bridges the rings, essentially isolating the Ce_{70} rings (figure 4). All bridging Ce^{IV}-monomers are fully occupied, showcasing a higher degree of sulfate ligation as compared to the CoCe$_{70}$-propeller, see Tables 1 and S9. This is observed in the higher number of chelating-bridging sulfates; most Ce^{IV}-monomers have one chelating sulfate. The Ce77 site has two chelating sulfates, and is 10-coordianted in a bicapped square-antiprismatic geometry. The Ce76 is also notably different. It only interacts with the neighboring ring on a chain via H-bonding of bound water, as it is mostly coordinated by aqua ligands. The lone Co^{II}-monomer site is fully coordinated by aqua ligands to charge balance and interact with the neighboring chains via H-bonding (figure S7).

The **ZnCe$_{70}$-Isolated** framework, formulated $[Zn(H_2O)_6]_{0.5}Ce_{4.5}Ce_{70}(OH)_{36}(O)_{64}(SO_4)_{67.5}(H_2O)_{64.75}$ (Table S8), crystallizes in the triclinic P-1 space group (V = 39,447 Å^3). This framework is isostructural with the Co-analogue. However, we

observe a diminished presence of Zn^{II}. Consequently, there is increased $Ce^{IV}-OSO_3$ ligation to compensate (Tables 1 and S9). This is marked by increased chelating sulfate and increased coordination number of the Ce^{IV}-monomer. The Zn^{II}-monomer has only a partial occupancy, of 0.5, limiting its interaction with the neighboring chains. As such, some partially occupied (0.25) Ce^{IV}-monomers bridge or interact via H-bonding of aqua ligands to the neighboring chains, presumably stabilizing interaction between the chains (figure S8).

Supramolecular assembly in organic media

As described for both the Ce_{70} and U_{70} solid-state frameworks, the role of the TM^{II} in the framework assembly depends on the ionic radius and preferred coordination environment (arising from the electronic configuration in the *d*-orbitals).[26, 59] Addenda sulfates also contribute to assembly, arguably the most important U_{70}-linker in the prior described U_{70}-family. In this new Ce_{70}-family, Ce^{IV}-monomers lead to differentiating assembly in the crystalline lattice. We prior reported the U_{70} frameworks dissolve in a butylamine-THF solvent mixture, and small-angle X-ray scattering (SAXS) shows supramolecular assembly in organic media is likewise mainly controlled by the addenda sulfates. The main observed species in this organic medium was a sulfate-linked offset dimer, $\{U_{70}\}_2$. The exception was Mn^{II}, which promoted the assembly of an eclipsed stack of eight rings, $\{U_{70}\}_8$. We attributed this prior to the competing TM-butylamine ligation—Mn^{II} has lesser tendency to bind the butylamine than the other transition metals.[67]
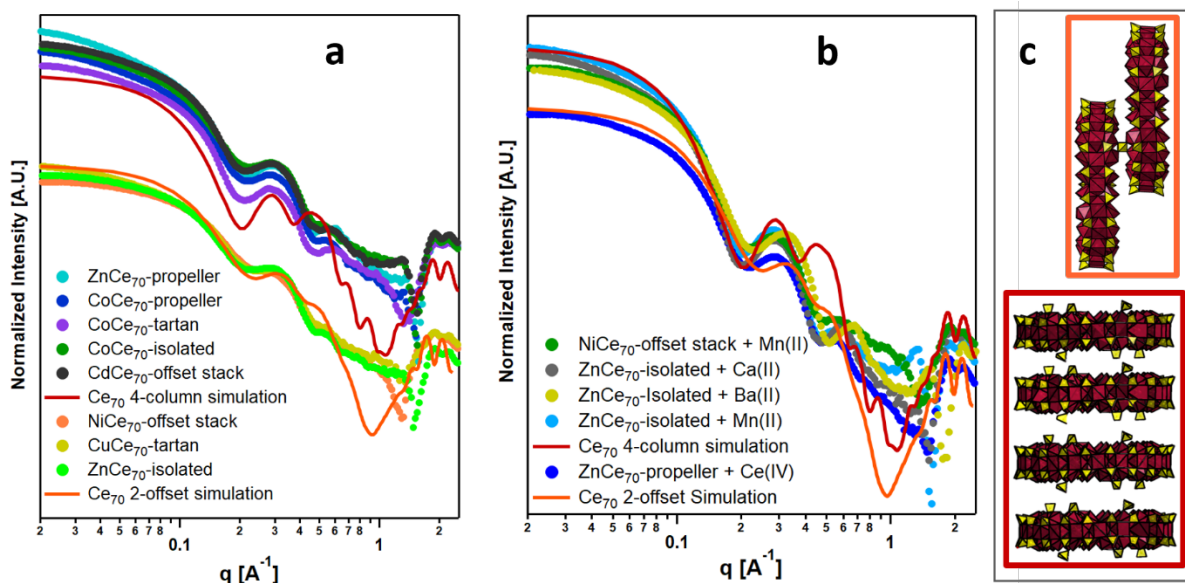
Figure 5. Small angle X-ray scattering of Ce$_{70}$ supramolecular assembly. a) Scattering curves for the eight reported structures, (5.0 mM, dissolved in 3:1 butylamine:tetrahydrofuran solvent mixture). b) Scattering curves for the ZnCe$_{70}$-structures with added Ba(II), Ca(II), Mn(II), and Ce(IV), and NiCe$_{70}$ offset-stack with added Mn(II). For both plots, scattering curves are offset for ease of viewing, and grouped with the simulated curve that they closest match (two Ce$_{70}$ exhibiting offset stacking, or four Ce$_{70}$ exhibiting eclipsed stacking, see part c). c) Polyhedral representation of two Ce$_{70}$-assemblies, for which scattering is simulated in parts a and b. The maroon box shows four eclipsed and stacked Ce$_{70}$ (simulated), and the orange box shows an offset dimer, observed in all Ce$_{70}$ frameworks. The box outline matches the color of the simulated scattering curves.

Here we show via SAXS studies that Ce$_{70}$ exhibits different stacking arrangements than U$_{70}$ in organic solvents, and the TM^{II} counterions play a more significant role. As identified in the solid state, there are four main architectural building blocks for the TMCe$_{70}$ frameworks; the Ce$_{70}$, the TM^{II} and Ce^{IV} monomers, and the ring-bridging sulfates. Upon dissolution in the organic media, the importance of these building units becomes evident (figure 5a). All solutions scatter strongly due to the heavy metal cerium and large aggregate size (intensity $\propto$ (atomic number)^2 and radius^6), allowing observation of oscillations, which differentiate varying Ce$_{70}$ arrangements. The dimensions of Ce$_{70}$ is ~33 Å diameter and ~4 Å height (Ce-Ce), where the majority of the scattering comes from the Ce-O core (figure S16).

To determine the size of dissolved Ce$_{70}$-aggregates, we first performed a size distribution analysis for each scattering curve, using a cylindrical (aspect ratio) model (parameters summarized in Table 2, data fitting shown in figures S10-S13). Two main sizes were observed for the eight reported phases. NiCe$_{70}$-offset stacking, CuCe$_{70}$-tartan, and ZnCe$_{70}$-isolated are a size equivalent to two Ce$_{70}$-units in an offset stack (figure 5c), both based on the dimensions of this dimer, and the similarity to the simulated scattering data (figure 5a). Notably, this is favored solution species observed for all TM^{II}-U$_{70}$ compounds.[59] The remaining five compounds; three Co-analogues, the CdCe$_{70}$-offset-stack, and the ZnCe$_{70}$-propeller are more consistent with a stack of four Ce$_{70}$ rings, eclipsed (Table 2, figure 5). Differences are noted amongst scattering curves within the two groups that are dominated by one or the other stacking arrangement (figure 5a). In particular, there is varying degree of increasing upward slope below q=0.1 Å^{-1}, owed to smaller concentrations of larger aggregates. This is also described by the size distribution data fitting, highlighted in figure S15.

The eclipsed Ce$_{70}$ 4-stack is unique compared to the prior TM^{II}-U$_{70}$ study. It is tempting to attribute this to linking via the Ce^{IV}-monomers (the U$_{70}$ phases do not have tetravalent monomers), but studies discussed below suggest just the opposite. In addition, the CdCe$_{70}$-offset-stack

framework dissolved as the eclipsed 4-stack, and it contains no Ce^{IV}-monomers. In Table 2, the dissolved compounds are organized from smallest to largest observed species, along with TM^{II} ionic radii (also in Table 1) to enable rationalization of trends. We observe a trend of larger TM^{II} promotes eclipsed stacking, suggesting the transition metals are responsible for linking Ce_{70} together into the eclipsed stack.

Table 2. Size Distribution Analysis of SAXS data

Crystal	TM^{II} Ionic Radius (Å)[2]	Aspect Ratio[1]	Cylinder diameter (Å)	Cylinder height (Å)	Peak Area	FWHM
dissolved Ce$_{70}$ frameworks						
offset stack (2-Ce$_{70}$)						
NiCe$_{70}$-offset-stacking	0.83	0.525	39.7	20.8	1.3	5.0
CuCe$_{70}$-tartan	0.87	0.525	40.7	21.4	4.0	4.0
ZnCe$_{70}$-isolated	0.88	0.525	42.6	22.4	2.5	4.2
eclipsed stack (4-Ce$_{70}$)						
ZnCe$_{70}$-propeller	0.88	1.75	35.3	61.8	3.3	3.5
CoCe$_{70}$-propeller	0.89	2	33.3	66.6	2.2	4.1
CdCe$_{70}$-offset-stacking	1.09	2	33.3	66.6	3.2	3.8
CoCe$_{70}$-isolated	0.89	2	34.1	68.2	2.5	3.5
CoCe$_{70}$-tartan	0.89	2	34.7	69.4	6.1	2.5
Ce$_{70}$ dissolved with added metal cations						
ZnCe$_{70}$-Propeller + Ce	1.01 (Ce^{IV})	0.525	45.1	23.7	2.9	3.6
ZnCe$_{70}$-Isolated + Mn	0.97 (Mn^{II})	2	36.4	72.8	7.6	1.7
ZnCe$_{70}$-Isolated + Ca	1.14 (Ca^{II})	2	36.6	73.2	5.4	2.4
ZnCe$_{70}$-Isolated + Ba	1.49 (Ba^{II})	2	38.4	76.8	27.7	0.4

[1]*aspect ratio=(cylinder height/cylinder diameter)*
[2]*six coordinate radius*[65]

The ZnCe$_{70}$-isolated and ZnCe$_{70}$-propeller present an interesting case; in the organic media, the former assembles as the offset dimer, and the latter assembles as the eclipsed 4-stack. The stark difference between these two frameworks is the isolated-framework contains far more Ce^{IV}-monomers (see Table 1). To further investigate the role of the Ce^{IV}-monomers (and other metal cations) on solution-phase assembly, we combined; 1) the ZnCe$_{70}$ isolated framework with Mn^{II}, Ca^{II} and Ba^{II}, and 2) the ZnCe$_{70}$-propeller framework with added Ce^{IV}. The resultant scattering

curves are shown in figure 5b, and the size distribution analysis summarized in Table 2 and figure S14. Interestingly, addition of Ce^{IV} to the $ZnCe_{70}$-propeller framework led to conversion of the larger eclipsed 4-stack (figure 5a) to the smaller offset dimer. This suggests that Ce^{IV} actually interferes with Ce_{70}-stacking. Based on the many solid-state characterizations of the Ce_{70} and U_{70} frameworks, we know the addenda sulfates play a considerable role in linking M_{70} to transition metals. In addition, these structures evidence the proclivity of sulfate bonding to hard tetravalent metal cations. Therefore, the role of the Ce^{IV}-monomers in preventing eclipsed stacking might be related for the tendency of these monomers to bind addenda sulfates in solution, preventing sulfate participation in extensive linking of Ce_{70}.

In contrast, Mn^{II}, Ca^{II} and Ba^{II} all converted the $ZnCe_{70}$-isolated framework from the offset dimer to the eclipsed 4-stack. In addition to the size-distribution analysis, we performed a core-shell cylinder fit of these latter three scattering curves, to assess if the added metal cation directly links the Ce_{70}-rings into the eclipsed stacks (figure S9 and Table S13). In the core-shell data analysis, the X-ray scattering length density of the solvent is set at 10×10^{10} cm^{-1} (rho, proportional to the electron density), and the rho-values for the shell (the Ce_{70}-ring stack plus any linking metals) and the core (inside the ring) are refined against the solvent value.[68] Indeed, we observe an increased rho-value from 99 to 110 to 206, for Ce_{70} solutions with added Ca, Mn and Ba, respectively. This is exactly consistent with the increasing number of electrons from 20 to 25 to 56 for Ca, Mn, and Ba respectively, providing compelling evidence that these metals are driving the solution phase connectivity from the offset dimer stack to the eclipsed 4-stack.

Summary and Outlook

Molecular cerium oxo-clusters are important for (1) understanding $Ce^{III/IV}$ catalysts, ion conductors and photoabsorbers, and (2) surrogate plutonium chemistry. Here we have introduced a new family of Ce^{IV} oxo-clusters, the Ce_{70} wheel is the largest to date, and the only one that does not grow symmetrically about the Ce_6 oxo-cluster core. The Ce^{IV}_{70} wheel is analogous to our prior reported U^{IV}_{70} wheel, hinting that this family could grow to include additional transitional metal and f-block M^{IV} members. Like the U_{70} family, Ce_{70} is isolated readily with TM^{II} counter-cations, and the addition of Ce^{IV}-monomers and addenda sulfates yields four intricate framework types. Dissolution of the frameworks in organic media and SAXS analysis reveals the role of lower valence metal cations (i.e. alkaline earths) on promoting supramolecular assembly and higher

valence metal cations (i.e. Ce^{IV}-monomers) on preventing assembly. Thus, in addition to the M^{IV}_{70} families crystallized from aqueous media, there is potential to surface-deposit M^{IV}_{70}-macrostructures from organic media with control over arrangement and connectivity of the rings. In addition to this ongoing effort, we are studying M^{IV}_{70} assembly pathways by isolating intermediates, crystallizing the Ln^{III}-Ce_{70} family, introducing Ce^{III} into the wheels via direct synthesis or electrochemistry, introducing organic linkers in attempt to grow M^{IV}_{70} MOFs, and translating the M^{IV}_{70} chemistry to Pu^{IV}. Outgrowth into these studies represents enormous potential for discovery of both fundamental and applied *f*-block and *d*-block M^{IV} oxo-cluster chemistry.

Experimental

Synthesis In the optimized experiments, we combined mixtures of the acetate and chloride salts of the various transition metals (see methods sections, SI). Optimized syntheses are summarized here, and details are provided in the SI, along with procedures for single-crystal X-ray diffraction, and SAXS. Bulk characterization including FTIR (Table S15, figure S17) and Raman (Table S16, figure S18) spectroscopies and PXRD (figures S19-S22) are also summarized in the SI. General synthesis of the **TMCe70** compounds entails the following. $Ce^{IV}(SO_4)_2$ (100 mg, 0.3 mmol) is dissolved in 500 µL H_2O in a 2 mL vial. The TM is introduced as optimized mixtures of $TM(Ac)_2$ plus $TMCl_2$. The vial is then placed in a sand bath and heated in an oven at 75 ˚C for 24 h. Crystalized products are then filtered and washed with water, followed by washing with 0.5 M HCl to remove any soluble byproduct or starting material.

Competing interests

The authors declare no competing interests

Additional information

Supplementary information is available for this paper at ….

References

1.   Sadeghi, O.; Zakharov, L. N.; Nyman, M., Aqueous formation and manipulation of the iron-oxo Keggin ion. *Science* **2015,** *347* (6228), 1359-1362.

2.   Weatherill, J. S.; Morris, K.; Bots, P.; Stawski, T. M.; Janssen, A.; Abrahamsen, L.; Blackham, R.; Shaw, S., Ferrihydrite Formation: The Role of Fe_{13} Keggin Clusters. *Environmental Science & Technology* **2016,** *50* (17), 9333-9342.

3.   Das, B., Theoretical Study of Small Iron–Oxyhydroxide Clusters and Formation of Ferrihydrite. *The Journal of Physical Chemistry A* **2018,** *122* (2), 652-661.

4.   Amiri, M.; Martin, N. P.; Sadeghi, O.; Nyman, M., Bismuth for Controlled Assembly/Disassembly of Transition-Metal Oxo Clusters, Defining Reaction Pathways in Inorganic Synthesis and Nature. *Inorganic Chemistry* **2020,** *59* (6), 3471-3481.

5.   Casey, W. H.; Rustad, J. R.; Banerjee, D.; Furrer, G., Large Molecules as Models for Small Particles in Aqueous Geochemistry Research. *Journal of Nanopraticle Research* **2005,** *7* (4-5), 377-387.

6.   Furrer, G., The Origin of Aluminum Flocs in Polluted Streams. *Science* **2002,** *297* (5590), 2245-2247.

7.   Fedeyko, J. M.; Vlachos, D. G.; Lobo, R. F., Formation and Structure of Self-Assembled Silica Nanoparticles in Basic Solutions of Organic and Inorganic Cations. *Langmuir* **2005,** *21* (11), 5197-5206.

8.   Xu, H.; Sommer, S.; Broge, N. L. N.; Gao, J.; Iversen, B. B., The Chemistry of Nucleation: In Situ Pair Distribution Function Analysis of Secondary Building Units During UiO-66 MOF Formation. *Chemistry – A European Journal* **2019,** *25* (8), 2051-2058.

9.   Soderholm, L.; Almond, P. M.; Skanthakumar, S.; Wilson, R. E.; Burns, P. C., The Structure of the Plutonium Oxide Nanocluster $[Pu_{38}O_{56}Cl_{54}(H_2O)_8]^{14-}$. *Angewandte Chemie International Edition* **2008,** *47* (2), 298-302.

10.   Chakraborty, B.; Weinstock, I. A., Water-soluble titanium-oxides: Complexes, clusters and nanocrystals. *Coordination Chemistry Reviews* **2019,** *382*, 85-102.

11.   Kozma, K.; Wang, M.; Molina, P. I.; Martin, N. P.; Feng, Z.; Nyman, M., The role of titanium-oxo clusters in the sulfate process for TiO_2 production. *Dalton Transactions* **2019,** *48* (29), 11086-11093.

12.   Sessoli, R.; Powell, A. K., Strategies towards single molecule magnets based on lanthanide ions. *Coordination Chemistry Reviews* **2009,** *253* (19-20), 2328-2341.

13.   Ako, A. M.; Hewitt, I. J.; Mereacre, V.; Clérac, R.; Wernsdorfer, W.; Anson, C. E.; Powell, A. K., A Ferromagnetically Coupled Mn_{19} Aggregate with a Record S=83/2 Ground Spin State. *Angewandte Chemie International Edition* **2006,** *45* (30), 4926-4929.

14.   Bagai, R.; Christou, G., The Drosophila of single-molecule magnetism: $[Mn_{12}O_{12}(O_2CR)_{16}(H_2O)_4]$. *Chemical Society Reviews* **2009,** *38* (4), 1011.

15.   Stroobants, K.; Moelants, E.; Ly, H. G. T.; Proost, P.; Bartik, K.; Parac-Vogt, T. N., Polyoxometalates as a Novel Class of Artificial Proteases: Selective Hydrolysis of Lysozyme under Physiological pH and Temperature Promoted by a Cerium(IV) Keggin-Type Polyoxometalate. *Chemistry - A European Journal* **2013,** *19* (8), 2848-2858.

16.   Chakraborty, B.; Gan-Or, G.; Duan, Y.; Raula, M.; Weinstock, I. A., Visible-Light-Driven Water Oxidation with a Polyoxometalate-Complexed Hematite Core of 275 Iron Atoms. *Angewandte Chemie International Edition* **2019,** *58* (20), 6584-6589.

17.   Tasiopoulos, A. J.; Vinslava, A.; Wernsdorfer, W.; Abboud, K. A.; Christou, G., Giant Single-Molecule Magnets: A{Mn_{84}} Torus and Its Supramolecular Nanotubes. *Angewandte Chemie International Edition* **2004,** *43* (16), 2117-2121.

18.   Moons, J.; Azambuja, F.; Mihailovic, J.; Kozma, K.; Smiljanic, K.; Amiri, M.; Cirkovic Velickovic, T.; Nyman, M.; Parac-Vogt, T. N., Discrete Hf_{18} Metal-oxo Cluster as a Heterogeneous Nanozyme for Site-Specific Proteolysis. *Angewandte Chemie International Edition* **2020,** *59* (23), 9094-9101.

19.   Liu, Y.; Howarth, A. J.; Vermeulen, N. A.; Moon, S.-Y.; Hupp, J. T.; Farha, O. K., Catalytic degradation of chemical warfare agents and their simulants by metal-organic frameworks. *Coordination Chemistry Reviews* **2017,** *346*, 101-111.

20.   Aulakh, D.; Liu, L.; Varghese, J. R.; Xie, H.; Islamoglu, T.; Duell, K.; Kung, C.-W.; Hsiung, C.-E.; Zhang, Y.; Drout, R. J.; Farha, O. K.; Dunbar, K. R.; Han, Y.; Wriedt, M., Direct Imaging of Isolated Single-Molecule Magnets in Metal–Organic Frameworks. *Journal of the American Chemical Society* **2019,** *141* (7), 2997-3005.

21.   Conic, D. P., K.; Parac-Vogt, T.; Harvey, J., Mechanism of the Highly Effective Peptide Bond Hydrolysis by MOF808 Catalyst Under Biologically Relevant Conditions. **2020**. Preprint (https://chemrxiv.org/articles/preprint/Mechanism_of_the_Highly_Effective_Peptide_Bond_Hydrolysis_ by_MOF808_Catalyst_Under_Biologically_Relevant_Conditions/12377648/1)

22.   Mitchell, S. G.; Streb, C.; Miras, H. N.; Boyd, T.; Long, D.-L.; Cronin, L., Face-directed self-assembly of an electronically active Archimedean polyoxometalate architecture. *Nature Chemistry* **2010,** *2* (4), 308-312.

23.   Xu, F.; Miras, H. N.; Scullion, R. A.; Long, D. L.; Thiel, J.; Cronin, L., Correlating the magic numbers of inorganic nanomolecular assemblies with a molecular-ring Rosetta Stone. **2012,** *109* (29), 11609-11612.

24.   Zhang, G.; Gadot, E.; Gan-Or, G.; Baranov, M.; Tubul, T.; Neyman, A.; Li, M.; Clotet, A.; Poblet, J. M.; Yin, P.; Weinstock, I. A., Self-Assembly and Ionic-Lattice-like Secondary Structure of a Flexible Linear Polymer of Highly Charged Inorganic Building Blocks. *Journal of the American Chemical Society* **2020,** *142* (16), 7295-7300.

25.   Claridge, S. A.; Castleman, A. W.; Khanna, S. N.; Murray, C. B.; Sen, A.; Weiss, P. S., Cluster-Assembled Materials. *ACS Nano* **2009,** *3* (2), 244-255.

26.   Colliard, I.; Morrison, G.; Loye, H.-C. Z.; Nyman, M., Supramolecular Assembly of U(IV) Clusters and Superatoms with Unconventional Countercations. *Journal of the American Chemical Society* **2020,** *142* (19), 9039-9047.

27.   Trovarelli, A., Catalytic Properties of Ceria and CeO_2-Containing Materials. *Catalysis Reviews* **1996,** *38* (4), 439-520.

28.   Fan, L.; Wang, C.; Chen, M.; Zhu, B., Recent development of ceria-based (nano)composite materials for low temperature ceramic fuel cells and electrolyte-free fuel cells. *Journal of Power Sources* **2013,** *234*, 154-174.

29.   Corma, A.; Atienzar, P.; García, H.; Chane-Ching, J.-Y., Hierarchically mesostructured doped CeO_2 with potential for solar-cell use. *Nature Materials* **2004,** *3* (6), 394-397.

30.   Paier, J.; Penschke, C.; Sauer, J., Oxygen Defects and Surface Chemistry of Ceria: Quantum Chemical Studies Compared to Experiment. *Chemical Reviews* **2013,** *113* (6), 3949-3985.

31.   Feng, W.; Sun, L.-D.; Zhang, Y.-W.; Yan, C.-H., Synthesis and assembly of rare earth nanostructures directed by the principle of coordination chemistry in solution-based process. *Coordination Chemistry Reviews* **2010,** *254* (9-10), 1038-1053.

32.   Lee, S. S.; Song, W.; Cho, M.; Puppala, H. L.; Nguyen, P.; Zhu, H.; Segatori, L.; Colvin, V. L., Antioxidant Properties of Cerium Oxide Nanocrystals as a Function of Nanocrystal Diameter and Surface Coating. *ACS Nano* **2013,** *7* (11), 9693-9703.

33.   Roulhac, P. L.; Palenik, G. J., Bond Valence Sums in Coordination Chemistry. The Calculation of the Oxidation State of Cerium in Complexes Containing Cerium Bonded Only to Oxygen. *Inorganic Chemistry* **2003,** *42* (1), 118-121.

34.   Das, R.; Sarma, R.; Baruah, J. B., A hexanuclear cerium(IV) cluster with mixed coordination environment. *Inorganic Chemistry Communications* **2010,** *13* (6), 793-795.

35.   Falaise, C.; Kozma, K.; Nyman, M., Thorium Oxo-Clusters as Building Blocks for Open Frameworks. *Chemistry - A European Journal* **2018,** *24,* 14226-14232.

36.   Cavka, J. H.; Jakobsen, S.; Olsbye, U.; Guillou, N.; Lamberti, C.; Bordiga, S.; Lillerud, K. P., A New Zirconium Inorganic Building Brick Forming Metal Organic Frameworks with Exceptional Stability. *Journal of the American Chemical Society* **2008,** *130* (42), 13850-13851.

37.   Knope, K. E.; Soderholm, L., Plutonium(IV) Cluster with a Hexanuclear $[Pu_6(OH)_4O_4]^{12+}$ Core. *Inorganic Chemistry* **2013,** *52* (12), 6770-6772.

38.   Martin, N. P.; Volkringer, C.; Henry, N.; Trivelli, X.; Stoclet, G.; Ikeda-Ohno, A.; Loiseau, T., Formation of a new type of uranium(iv) poly-oxo cluster {U_{38}} based on a controlled release of water via esterification reaction. *Chemical Science* **2018,** *9* (22), 5021-5032.

39.   Kalaji, A.; Soderholm, L., Aqueous Hafnium Sulfate Chemistry: Structures of Crystalline Precipitates. *Inorganic Chemistry* **2014,** *53* (20), 11252-11260.

40.   Falaise, C.; Neal, H. A.; Nyman, M., U(IV) Aqueous Speciation from the Monomer to UO_2 Nanoparticles: Two Levels of Control from Zwitterionic Glycine Ligands. *Inorganic Chemistry* **2017,** *56* (11), 6591-6598.

41.   Dufaye, M.; Duval, S.; Stoclet, G.; Loiseau, T., Influence of pH on Ce^{IV}-$[As^{III}W_9O_{33}]^{9-}$ association for the formation of hexanuclear cerium(iv) oxo-hydroxo-clusters stabilized by trivacant polyanions. *CrystEngComm* **2020,** *22* (2), 371-380.

42.   Duval, S.; Roussel, P.; Loiseau, T., Synthesis of a large dodecameric cerium cluster stabilized by the $[SiW_9O_{34}]^{10-}$ polyoxometalate. *Inorganic Chemistry Communications* **2017,** *83*, 52-54.

43.   Duval, S.; Trivelli, X.; Roussel, P.; Loiseau, T., Influence of the pH on the Condensation of Tetravalent Cerium Cations in Association with $[\alpha\text{-}SiW_9O_{34}]^{10-}$ Leading to the Formation of a $Ce_6O_4(OH)_4$ Core. *European Journal of Inorganic Chemistry* **2016,** *2016* (34), 5373-5379.

44.   Malaestean, I. L.; Ellern, A.; Baca, S.; Kögerler, P., Cerium oxide nanoclusters: commensurate with concepts of polyoxometalate chemistry? *Chemistry Communications* **2012,** *48* (10), 1499-1501.

45.   Estes, S. L.; Antonio, M. R.; Soderholm, L., Tetravalent Ce in the Nitrate-Decorated Hexanuclear Cluster $[Ce_6(\mu_3\text{-}O)_4(\mu_3\text{-}OH)_4]^{12+}$: A Structural Endpoint for Ceria Nanoparticles. *Journal of Physical Chemistry C* **2016,** *120* (10), 5810-5818.

46.   Mathey, L.; Paul, M.; Copéret, C.; Tsurugi, H.; Mashima, K., Cerium(IV) Hexanuclear Clusters from Cerium(III) Precursors: Molecular Models for Oxidative Growth of Ceria Nanoparticles. *Chemistry - A European Journal* **2015,** *21* (38), 13454-13461.

47.   Lundgren, G., The structures of oxide and hydroxide salts of some tetrapositive ions. *Recueil des Travaux Chimiques des Pays-Bas* **1956,** *75* (5), 585-588.

48.   Toledano, P.; Ribot, F.; Sanchez, C., *Seance Academie Science* **1990,** *2* (331), 1315.

49.   Lammert, M.; Wharmby, M. T.; Smolders, S.; Bueken, B.; Lieb, A.; Lomachenko, K. A.; Vos, D. D.; Stock, N., Cerium-based metal organic frameworks with UiO-66 architecture: synthesis, properties and redox catalytic activity. *Chemical Communications* **2015,** *51* (63), 12578-12581.

50.   Lammert, M.; Glißmann, C.; Reinsch, H.; Stock, N., Synthesis and Characterization of New Ce(IV)-MOFs Exhibiting Various Framework Topologies. *Crystal Growth & Design* **2017,** *17* (3), 1125-1131.

51.   Zhang, Y.-F.; Wang, Q.; Xue, D.-X.; Bai, J., Single-Crystal Synthesis and Diverse Topologies of Hexanuclear CeIV-Based Metal–Organic Frameworks. *Inorganic Chemistry* **2020,** *59* (16), 11233-11237.

52.   Hennig, C.; Ikeda-Ohno, A.; Kraus, W.; Weiss, S.; Pattison, P.; Emerich, H.; Abdala, P. M.; Scheinost, A. C., Crystal Structure and Solution Species of Ce(III) and Ce(IV) Formates: From Mononuclear to Hexanuclear Complexes. *Inorganic Chemistry* **2013,** *52* (20), 11734-11743.

53.   Matsunaga, S.; Inoue, Y.; Mihara, K.; Nomiya, K., Synthesis and crystal structure of hexacerium(IV) cluster-containing Keggin polyoxometalate trimer. *Inorganic Chemistry Communications* **2017,** *80*, 61-64.

54.   Qasim, H. M.; Ayass, W. W.; Donfack, P.; Mougharbel, A. S.; Bhattacharya, S.; Nisar, T.; Balster, T.; Solé-Daura, A.; Römer, I.; Goura, J.; Materny, A.; Wagner, V.; Poblet, J. M.; Bassil, B. S.; Kortz, U., Peroxo-Cerium(IV)-Containing Polyoxometalates: $[Ce^{IV}_6(O_2)_9(GeW_{10}O_{37})_3]^{24-}$, a Recyclable Homogeneous Oxidation Catalyst. *Inorganic Chemistry* **2019,** *58* (17), 11300-11307.

55.   Mitchell, K. J.; Abboud, K. A.; Christou, G., Atomically-precise colloidal nanoparticles of cerium dioxide. *Nature Communications* **2017,** *8* (1), 1-7.

56.   Sigmon, G. E.; Hixon, A. E., Extension of the Plutonium Oxide Nanocluster Family to Include {Pu$_{16}$} and {Pu$_{22}$}. *Chemistry – A European Journal* **2019,** *25* (10), 2463-2466.

57.   Sweet, L. E.; Corbey, J. F.; Gendron, F.; Autschbach, J.; McNamara, B. K.; Ziegelgruber, K. L.; Arrigo, L. M.; Peper, S. M.; Schwantes, J. M., Structure and Bonding Investigation of Plutonium Peroxocarbonate Complexes Using Cerium Surrogates and Electronic Structure Modeling. *Inorganic Chemistry* **2017,** *56* (2), 791-801.

58.   Wilson, R. E.; Skanthakumar, S.; Soderholm, L., Separation of Plutonium Oxide Nanoparticles and Colloids. *Angewandte Chemie International Edition* **2011,** *50* (47), 11234-11237.

59.   Colliard, I.; Nyman, M., Building $[U^{IV}_{70}(OH)_{36}(O)_{64}]^{4-}$ oxocluster frameworks with sulfate, transition metals, and UV. *Chemistry – A European Journal* **2020,** *26,* 1-9.

60.   Cardenas, E.; Wu, W. M.; Leigh, M. B.; Carley, J.; Carroll, S.; Gentry, T.; Luo, J.; Watson, D.; Gu, B.; Ginder-Vogel, M.; Kitanidis, P. K.; Jardine, P. M.; Zhou, J.; Criddle, C. S.; Marsh, T. L.; Tiedje, J. M., Significant Association between Sulfate-Reducing Bacteria and Uranium-Reducing

Microbial Communities as Revealed by a Combined Massively Parallel Sequencing-Indicator Species Approach. *American Society for Microbiology* **2010,** *76* (20), 6778-6786.

61.   Chen, L.; Turo, M. J.; Gembicky, M.; Reinicke, R. A.; Schimpf, A. M., Cation-Controlled Assembly of Polyoxotungstate-Based Coordination Networks. *Angewandte Chemie International Edition* **2020,** *59*, 2-9.

62.   Chen, H.; Tu, H.; Hu, C.; Liu, Y.; Dong, D.; Sun, Y.; Dai, Y.; Wang, S.; Qian, H.; Lin, Z.; Chen, L., Cationic Covalent Organic Framework Nanosheets for Fast Li-Ion Conduction. *Journal of the American Chemical Society* **2018,** *140* (3), 896-899.

63.   Bernasconi, L.; Fois, E.; Selloni, A., Cation–anion versus cation–framework interactions in sodalites: First-principles study of model Cu-exchanged sodalites. **1999,** *110* (18), 9048.

64.   Misra, A.; Kozma, K.; Streb, C.; Nyman, M., Beyond Charge Balance: Counter-Cations in Polyoxometalate Chemistry. *Angewandte Chemie International Edition* **2020,** *59* (2), 596-612.

65.   Shannon, R., Revised effective ionic radii and systematic studies of interatomic distances in halides and chalcogenides. *Acta Crystallographica Section A* **1976,** *32* (5), 751-767.

66.   Frank, P.; Szilagyi, R. K.; Gramlich, V.; Hsu, H.-F.; Hedman, B.; Hodgson, K. O., Spin-Polarization-Induced Preedge Transitions in the Sulfur K-Edge XAS Spectra of Open-Shell Transition-Metal Sulfates: Spectroscopic Validation of σ-Bond Electron Transfer. *Inorganic Chemistry* **2017,** *56* (3), 1080-1093.

67.   Mishustin, A. I., Formation constants for complexes of transition-metal cations with O- and N-donor ligands in aqueous solutions. *Russian Journal of Inorganic Chemistry* **2007,** *52* (2), 283-288.

68.   Ilavsky, J.; Jemian, P. R., Irena: tool suite for modeling and analysis of small-angle scattering. *Journal of Applied Crystallography* **2009,** *42* (2), 347-353.

For table of contents only